

Introduction to Photonic Crystals: Bloch's Theorem, Band Diagrams, and Gaps (But No Defects)

Steven G. Johnson and J. D. Joannopoulos, MIT

3rd February 2003

1 Introduction

Photonic crystals are periodically structured electromagnetic media, generally possessing *photonic band gaps*: ranges of frequency in which light cannot propagate through the structure. This periodicity, whose lengthscale is proportional to the wavelength of light in the band gap, is the electromagnetic analogue of a crystalline atomic lattice, where the latter acts on the electron wavefunction to produce the familiar band gaps, semiconductors, and so on, of solid-state physics. The study of photonic crystals is likewise governed by the Bloch-Floquet theorem, and intentionally introduced defects in the crystal (analogous to electronic dopants) give rise to localized electromagnetic states: linear waveguides and point-like cavities. The crystal can thus form a kind of perfect optical “insulator,” which can confine light losslessly around sharp bends, in lower-index media, and within wavelength-scale cavities, among other novel possibilities for control of electromagnetic phenomena. Below, we introduce the basic theoretical background of photonic crystals in one, two, and three dimensions (schematically depicted in Fig. 1), as well as hybrid structures that combine photonic-crystal effects in some directions with more-conventional index guiding in other directions. (Line and point defects in photonic crystals are discussed elsewhere.)

Electromagnetic wave propagation in periodic media was first studied by Lord Rayleigh in 1887, in connection with the peculiar reflective properties of a crystalline mineral with periodic “twinning” planes (across which the dielectric tensor undergoes a mirror flip). These correspond to one-dimensional photonic crystals, and he identified the fact that they have a narrow band gap prohibiting light propagation through the planes. This band gap is angle-dependent, due to the differing periodicities experienced by light propagating at non-normal incidences, producing a reflected color that varies sharply with angle. (A similar effect is responsible for many other iridescent colors in nature, such as butterfly wings and abalone shells.) Although multilayer films received intensive study

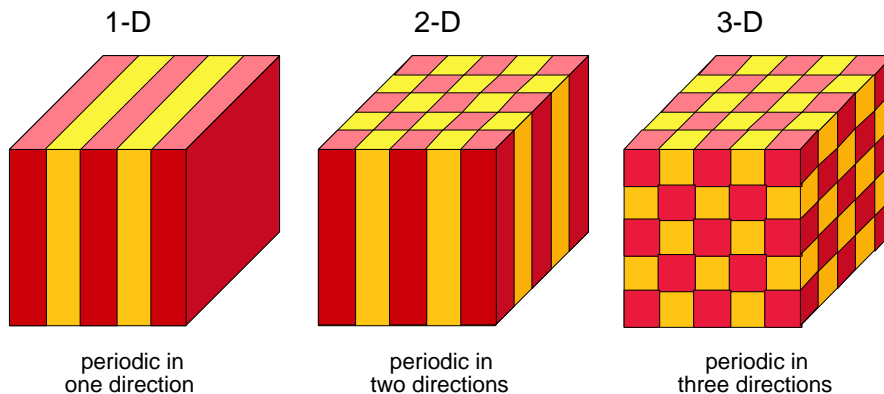


Figure 1: Schematic depiction of photonic crystals periodic in one, two, and three directions, where the periodicity is in the material (typically dielectric) structure of the crystal. Only a 3d periodicity, with a more complex topology than is shown here, can support an omnidirectional photonic bandgap

over the following century, it was not until 100 years later, when Yablonovitch and John in 1987 joined the tools of classical electromagnetism and solid-state physics, that the concepts of omnidirectional photonic band gaps in two and three dimensions was introduced. This generalization, which inspired the name “photonic crystal,” led to many subsequent developments in their fabrication, theory, and application, from integrated optics to negative refraction to optical fibers that guide light in air.

2 Maxwell’s Equations in Periodic Media

The study of wave propagation in three-dimensionally periodic media was pioneered by Felix Bloch in 1928, unknowingly extending an 1883 theorem in one dimension by G. Floquet. Bloch proved that waves in such a medium can propagate without scattering, their behavior governed by a periodic envelope function multiplied by a planewave. Although Bloch studied quantum mechanics, leading to the surprising result that electrons in a conductor scatter only from imperfections and not from the periodic ions, the same techniques can be applied to electromagnetism by casting Maxwell’s equations as an eigenproblem in analogue with Schrödinger’s equation. By combining the source-free Faraday’s and Ampere’s laws at a fixed frequency ω , *i.e.* time dependence $e^{-i\omega t}$, one can obtain an equation in only the magnetic field \vec{H} :

$$\vec{\nabla} \times \frac{1}{\varepsilon} \vec{\nabla} \times \vec{H} = \left(\frac{\omega}{c}\right)^2 \vec{H}, \quad (1)$$

where ε is the dielectric function $\varepsilon(x, y, z)$ and c is the speed of light. This is an eigenvalue equation, with eigenvalue $(\omega/c)^2$ and an eigen-operator $\vec{\nabla} \times$

$\frac{1}{\varepsilon}\vec{\nabla}\times$ that is *Hermitian* (acts the same to the left and right) under the inner product $\int \vec{H}^* \cdot \vec{H}'$ between two fields \vec{H} and \vec{H}' . (The two curls correspond roughly to the “kinetic energy” and $1/\varepsilon$ to the “potential” compared to the Schrödinger Hamiltonian $\nabla^2 + V$.) It is sometimes more convenient to instead write a *generalized* Hermitian eigenproblem in the electric field \vec{E} , $\vec{\nabla}\times\vec{\nabla}\times\vec{E} = (\omega/c)^2\varepsilon\vec{E}$, which separates the kinetic and potential terms. Electric fields that lie in higher ε , *i.e.* lower potential, will have lower ω ; this is discussed further in the context of the variational theorem of Eq. (3).

Thus, the same linear-algebraic theorems as those in quantum mechanics can be applied to the electromagnetic wave solutions. The fact that the eigenoperator is Hermitian and positive-definite (for real $\varepsilon > 0$) implies that the eigenfrequencies ω are real, for example, and also leads to orthogonality, variational formulations, and perturbation-theory relations that we discuss further below. An important difference compared to quantum mechanics is that there is a *transversality constraint*: one typically excludes $\vec{\nabla}\cdot\vec{H} \neq 0$ (or $\vec{\nabla}\cdot\varepsilon\vec{E} \neq 0$) eigensolutions, which lie at $\omega = 0$; *i.e.* static-field solutions with free magnetic (or electric) charge are forbidden.

2.1 Bloch waves and Brillouin zones

A photonic crystal corresponds to a periodic dielectric function $\varepsilon(\vec{x}) = \varepsilon(\vec{x} + \vec{R}_i)$ for some *primitive lattice vectors* \vec{R}_i ($i = 1, 2, 3$ for a crystal periodic in all three dimensions). In this case, the Bloch-Floquet theorem for periodic eigenproblems states that the solutions to Eq. (1) can be chosen of the form $\vec{H}(\vec{x}) = e^{i\vec{k}\cdot\vec{x}}\vec{H}_{n,\vec{k}}(\vec{x})$ with eigenvalues $\omega_n(\vec{k})$, where $\vec{H}_{n,\vec{k}}$ is a *periodic* envelope function satisfying:

$$(\vec{\nabla} + i\vec{k}) \times \frac{1}{\varepsilon}(\vec{\nabla} + i\vec{k}) \times \vec{H}_{n,\vec{k}} = \left(\frac{\omega_n(\vec{k})}{c}\right)^2 \vec{H}_{n,\vec{k}}, \quad (2)$$

yielding a different Hermitian eigenproblem over the primitive cell of the lattice at each Bloch wavevector \vec{k} . This primitive cell is a finite domain if the structure is periodic in all directions, leading to discrete eigenvalues labelled by $n = 1, 2, \dots$. These eigenvalues $\omega_n(\vec{k})$ are continuous functions of \vec{k} , forming discrete “bands” when plotted versus the latter, in a “band structure” or dispersion diagram—both ω and \vec{k} are conserved quantities, meaning that a band diagram maps out all possible interactions in the system. (Note also that \vec{k} is not required to be real; complex \vec{k} gives evanescent modes that can exponentially decay from the boundaries of a finite crystal, but which cannot exist in the bulk.)

Moreover, the eigensolutions are periodic functions of \vec{k} as well: the solution at \vec{k} is the same as the solution at $\vec{k} + \vec{G}_j$, where \vec{G}_j is a primitive *reciprocal lattice vector* defined by $\vec{R}_i \cdot \vec{G}_j = 2\pi\delta_{i,j}$. Thanks to this periodicity, one need only compute the eigensolutions for \vec{k} within the primitive cell of this reciprocal

lattice—or, more conventionally, one considers the set of inequivalent wavevectors closest to the $\vec{k} = 0$ origin, a region called the first Brillouin zone. For example, in a one-dimensional system, where $R_1 = a$ for some periodicity a and $G_1 = 2\pi/a$, the first Brillouin zone is the region $k = -\frac{\pi}{a} \dots \frac{\pi}{a}$; all other wavevectors are equivalent to some point in this zone under translation by a multiple of G_1 . Furthermore, the first Brillouin zone may itself be redundant if the crystal possesses additional symmetries such as mirror planes; by eliminating these redundant regions, one obtains the *irreducible Brillouin zone*, a convex polyhedron that can be found tabulated for most crystalline structures. In the preceding one-dimensional example, since most systems will have time-reversal symmetry ($k \rightarrow -k$), the irreducible Brillouin zone would be $k = 0 \dots \frac{\pi}{a}$.

The familiar dispersion relations of uniform waveguides arise as a special case of the Bloch formalism: such translational symmetry corresponds to a period $a \rightarrow 0$. In this case, the Brillouin zone of the wavevector k (also called β) is unbounded, and the envelope function $\vec{H}_{n,k}$ is a function only of the transverse coordinates.

2.2 The origin of the photonic band gap

A complete photonic band gap is a range of ω in which there are no propagating (real \vec{k}) solutions of Maxwell's equations (2) for any \vec{k} , surrounded by propagating states above and below the gap. There are also incomplete gaps, which only exist over a subset of all possible wavevectors, polarizations, and/or symmetries. We discuss both sorts of gaps in the subsequent sections, but in either case their origins are the same, and can be understood by examining the consequences of periodicity for a simple one-dimensional system.

Consider a one-dimensional system with uniform $\varepsilon = 1$, which has plane-wave eigensolutions $\omega(k) = ck$, as depicted in Fig. 1(left). This ε has trivial periodicity a for any $a \geq 0$, with $a = 0$ giving the usual unbounded dispersion relation. We are free, however, to label the states in terms of Bloch envelope functions and wavevectors for some $a \neq 0$, in which case the bands for $|k| > \pi/a$ are translated (“folded”) into the first Brillouin zone, as shown by the dashed lines in Fig. 2(left). In particular, the $k = -\pi/a$ mode in this description now lies at an equivalent wavevector to the $k = \pi/a$ mode, and at the same frequency; this accidental degeneracy is an artifact of the “artificial” period we have chosen. Instead of writing these wave solutions with electric fields $\vec{E}(x) \sim e^{\pm i\pi x/a}$, we can equivalently write linear combinations $e(x) = \cos(\pi x/a)$ and $o(x) = \sin(\pi x/a)$ as shown in Fig. 3, both at $\omega = c\pi/a$. Now, however, suppose that we perturb ε so that it is nontrivially periodic with period a ; for example, a sinusoid $\varepsilon(x) = 1 + \Delta \cdot \cos(2\pi x/a)$, or a square wave as in the inset of Fig. 2. In the presence of such an oscillating “potential,” the accidental degeneracy between $e(x)$ and $o(x)$ is broken: supposing $\Delta > 0$, then the field $e(x)$ is more concentrated in the higher- ε regions than $o(x)$, and so lies at a lower frequency. This opposite shifting of the bands creates a band gap, as depicted in Fig. 2(right). (In fact, from the perturbation theory described subsequently, one can show that for $\Delta \ll 1$ the band gap, as a fraction of mid-gap frequency, is $\Delta\omega/\omega \cong \Delta/2$.)

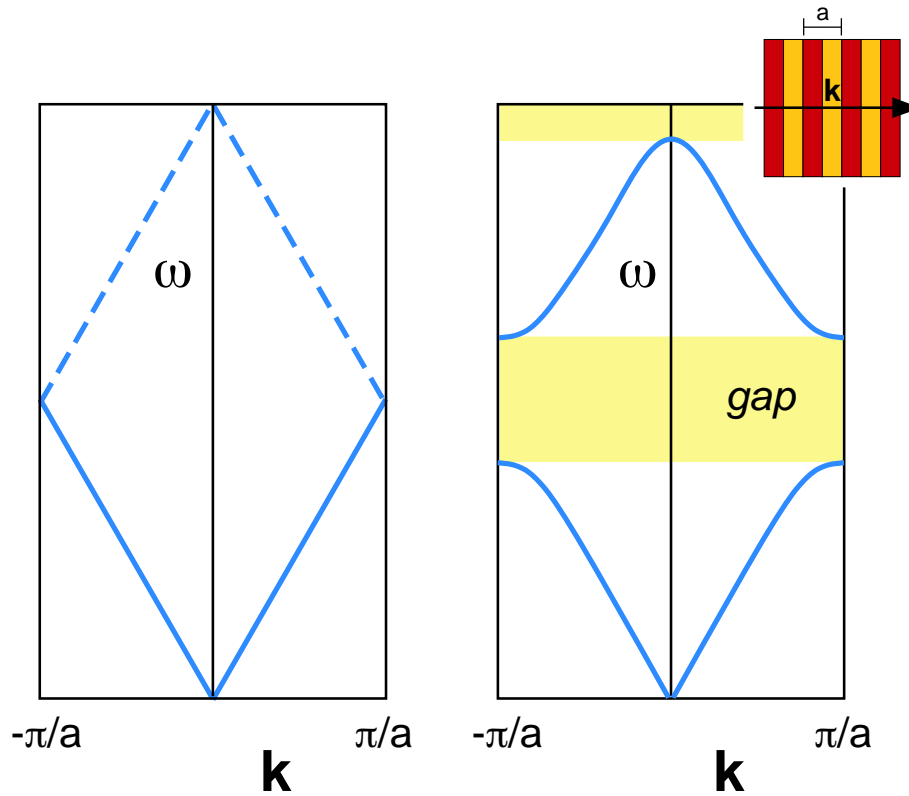


Figure 2: Left: Dispersion relation (band diagram), frequency ω versus wavenumber k , of a uniform one-dimensional medium, where the dashed lines show the “folding” effect of applying Bloch’s theorem with an artificial periodicity a . Right: Schematic effect on the bands of a physical periodic dielectric variation (inset), where a gap has been opened by splitting the degeneracy at the $k = \pm\pi/a$ Brillouin-zone boundaries (as well as a higher-order gap at $k = 0$).

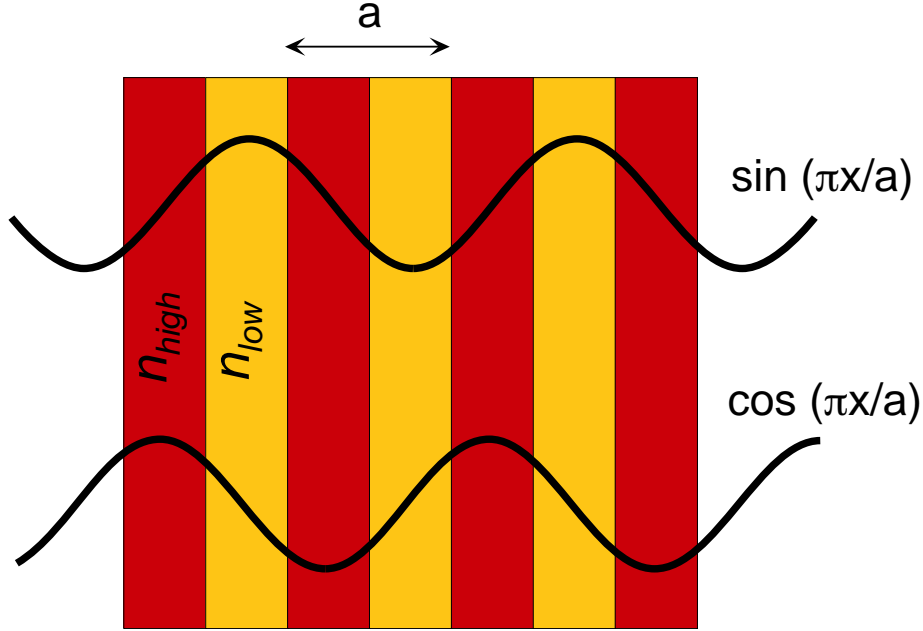


Figure 3: Schematic origin of the band gap in one dimension. The degenerate $k = \pm\pi/a$ plane waves of a uniform medium are split into $\cos(\pi x/a)$ and $\sin(\pi x/a)$ standing waves by a dielectric periodicity, forming the lower and upper edges of the band gap, respectively—the former has electric-field peaks in the high dielectric (n_{high}) and so will lie at a lower frequency than the latter (which peaks in the low dielectric).

By the same arguments, it follows that *any* periodic dielectric variation in one dimension will lead to a band gap, albeit a small gap for a small variation; a similar result was identified by Lord Rayleigh in 1887.

More generally, it follows immediately from the properties of Hermitian eigensystems that the eigenvalues minimize a *variational problem*:

$$\omega_{n,\vec{k}}^2 = \min_{\vec{E}_{n,\vec{k}}} \frac{\int |(\vec{\nabla} + i\vec{k}) \times \vec{E}_{n,\vec{k}}|^2}{\int \varepsilon |\vec{E}_{n,\vec{k}}|^2} c^2, \quad (3)$$

in terms of the periodic electric field envelope $\vec{E}_{n,\vec{k}}$, where the numerator minimizes the “kinetic energy” and the denominator minimizes the “potential energy.” Here, the $n > 1$ bands are additionally constrained to be orthogonal to the lower bands:

$$\int \vec{H}_{m,\vec{k}}^* \cdot \vec{H}_{n,\vec{k}} = \int \varepsilon \vec{E}_{m,\vec{k}}^* \cdot \vec{E}_{n,\vec{k}} = 0 \quad (4)$$

for $m < n$. Thus, at each \vec{k} , there will be a gap between the lower “dielectric”

bands concentrated in the high dielectric (low potential) and the upper “air” bands that are less concentrated in the high dielectric: the air bands are forced out by the orthogonality condition, or otherwise must have fast oscillations that increase their kinetic energy. (The dielectric/air bands are analogous to the valence/conduction bands in a semiconductor.)

In order for a complete band gap to arise in two or three dimensions, two additional hurdles must be overcome. First, although in each symmetry direction of the crystal (and each \vec{k} point) there will be a band gap by the one-dimensional argument, these band gaps will not necessarily overlap in frequency (or even lie between the same bands). In order that they overlap, the gaps must be sufficiently large, which implies a minimum ε contrast (typically at least 4/1 in 3d). Since the 1d mid-gap frequency $\sim c\pi/a\sqrt{\varepsilon}$ varies inversely with the period a , it is also helpful if the periodicity is nearly the same in different directions—thus, the largest gaps typically arise for hexagonal lattices in 2d and fcc lattices in 3d, which have the most nearly circular/spherical Brillouin zones. Second, one must take into account the vectorial boundary conditions on the electric field: moving across a dielectric boundary from ε to some $\varepsilon' < \varepsilon$, the inverse “potential” $\varepsilon|\vec{E}|^2$ will *decrease* discontinuously if \vec{E} is parallel to the interface (\vec{E}_{\parallel} is continuous) and will *increase* discontinuously if \vec{E} is perpendicular to the interface ($\varepsilon\vec{E}_{\perp}$ is continuous). This means that, whenever the electric field lines cross a dielectric boundary, it is much harder to strongly contain the field energy within the high dielectric, and the converse is true when the field lines are parallel to a boundary. Thus, in order to obtain a large band gap, a dielectric structure should consist of thin, continuous veins/membranes along which the electric field lines can run—this way, the lowest band(s) can be strongly confined, while the upper bands are forced to a much higher frequency because the thin veins cannot support multiple modes (except for two orthogonal polarizations). The veins must also run in all directions, so that this confinement can occur for all \vec{k} and polarizations, necessitating a complex topology in the crystal.

Ultimately, however, in two or three dimensions we can only suggest rules of thumb for the existence of a band gap in a periodic structure, since no rigorous criteria have yet been determined. This made the design of 3d photonic crystals a trial and error process, with the first example by Ho *et al.* of a complete 3d gap coming three years after the initial 1987 concept. As is discussed by the final section below, a small number of families of 3d photonic crystals have since been identified, with many variations thereof explored for fabrication.

2.3 Computational techniques

Because photonic crystals are generally complex, high index-contrast, two- and three-dimensional vectorial systems, numerical computations are a crucial part of most theoretical analyses. Such computations typically fall into three categories: time-domain “numerical experiments” that model the time-evolution of the fields with arbitrary starting conditions in a discretized system (*e.g.* finite-difference); definite-frequency transfer matrices wherein the scattering matri-

ces are computed in some basis to extract transmission/reflection through the structure; and frequency-domain methods to directly extract the Bloch fields and frequencies by diagonalizing the eigenoperator. The first two categories intuitively correspond to directly measurable quantities such as transmission (although they can also be used to compute *e.g.* eigenvalues), whereas the third is more abstract, yielding the band diagrams that provide a guide to interpretation of measurements as well as a starting-point for device design and semi-analytical methods. Moreover, several band diagrams are included in the following sections, and so we briefly outline the frequency-domain method used to compute them.

Any frequency-domain method begins by expanding the fields in some complete basis, $\vec{H}_{\vec{k}}(\vec{x}) = \sum_n h_n \vec{b}_n(\vec{x})$, transforming the partial differential equation (2) into a discrete matrix eigenvalue problem for the coefficients h_n . Truncating the basis to N elements leads to $N \times N$ matrices, which could be diagonalized in $O(N^3)$ time by standard methods. This is impractical for large 3d systems, however, and is also unnecessary—typically, one only wants the few lowest eigenfrequencies, in which case one can use iterative eigensolver methods requiring only $\sim O(N)$ time. Perhaps the simplest such method is based directly on the variational theorem (3): given some starting coefficients h_n , one iteratively minimizes the variational (“Rayleigh”) quotient using *e.g.* preconditioned conjugate-gradient descent. This yields the lowest band’s eigenvalue and field, and upper bands are found by the same minimization while orthogonalizing against the lower bands (“deflation”). There is one additional difficulty, however, and that is that one must at the same time enforce the $(\vec{\nabla} + i\vec{k}) \cdot \vec{H}_{\vec{k}} = 0$ transversality constraint, which is nontrivial in three dimensions. The simplest way to maintain this constraint is to employ a basis that is already transverse, for example planewaves $\vec{h}_{\vec{G}} e^{i\vec{G} \cdot \vec{x}}$ with transverse amplitudes $\vec{h}_{\vec{G}} \cdot (\vec{G} + \vec{k}) = 0$. (In such a planewave basis, the action of the eigen-operator can be computed via a fast Fourier transform in $O(N \log N)$ time.)

2.4 Semi-analytical methods: perturbation theory

As in quantum mechanics, the eigenstates can be the starting point for many analytical and semi-analytical studies. One common technique is perturbation theory, applied to small deviations from an ideal system—closely related to the variational expression (3), perturbation theory can be exploited to consider effects such as nonlinearities, material absorption, fabrication disorder, and external tunability. Not only is perturbation theory useful in its own right, but it also illustrates both old and peculiarly new features that arise in such analyses of electromagnetism compared to scalar problems such as quantum mechanics.

Given an unperturbed eigenfield $\vec{E}_{n,\vec{k}}$ for a structure ε , the lowest-order correction $\Delta\omega_n^{(1)}$ to the eigenfrequency from a small perturbation $\Delta\varepsilon$ is given

by:

$$\Delta\omega_n^{(1)} = -\frac{\omega_n(\vec{k})}{2} \frac{\int \Delta\varepsilon |\vec{E}_{n,\vec{k}}|^2}{\int \varepsilon |\vec{E}_{n,\vec{k}}|^2}, \quad (5)$$

where the integral is over the primitive cell of the lattice. A Kerr nonlinearity would give $\Delta\varepsilon \sim |\vec{E}|^2$, material absorption would produce an imaginary frequency correction (decay coefficient) from a small imaginary $\Delta\varepsilon$, and so on. Similarly, one can compute the shift in frequency from a small $\Delta\vec{k}$ in order to determine the group velocity $d\omega/dk$; this variation of perturbation theory is also called $k \cdot p$ theory. All such first-order perturbation corrections are well known from quantum mechanics, and in the limit of infinitesimal perturbations give the exact Hellman-Feynman expression for the derivative of the eigenvalue. However, in the limit where $\Delta\varepsilon$ is a small shift Δh of a dielectric boundary between some ε_1 and ε_2 , an important class of geometric perturbation, Eq. (5) gives a surface integral of $|\vec{E}|^2$ on the interface, but this is *ill-defined* because the field there is discontinuous. The proper derivation of perturbation theory in the face of such discontinuity requires a more careful limiting process from an anisotropically smoothed system, yielding the surface integral:

$$\Delta\omega_n^{(1)} = -\frac{\omega_n(\vec{k})}{2} \frac{\iint \Delta h \left(\Delta\varepsilon_{12} |\vec{E}_{\parallel}|^2 - \Delta\varepsilon_{12}^{-1} |D_{\perp}|^2 \right)}{\int \varepsilon |\vec{E}_{n,\vec{k}}|^2},$$

where $\Delta\varepsilon_{12} = \varepsilon_1 - \varepsilon_2$, $\Delta\varepsilon_{12}^{-1} = \varepsilon_1^{-1} - \varepsilon_2^{-1}$, and $\vec{E}_{\parallel}/D_{\perp}$ denotes the (continuous) interface parallel/perpendicular components of the unperturbed electric/displacement eigenfield. A similar expression is required in high index-contrast systems to employ, *e.g.*, coupled-mode theory for slowly-varying waveguides or Green's functions for interface roughness.

Standard perturbation-theory techniques also provide expressions for higher-order corrections to the eigenvalue and eigenfield, based on an expansion in the basis of the unperturbed eigenfields. This approach, however, runs into immediate difficulty because the eigenfields are also subject to the transversality constraint, $(\vec{\nabla} + i\vec{k}) \cdot \varepsilon \vec{E}_{\vec{k}} = 0$, and this constraint varies with ε and \vec{k} —the eigenfields $\vec{E}_{\vec{k}}$ are not a complete basis for the eigenfields constrained at a different ε or \vec{k} . For ε perturbations, this problem can be eliminated by using the \vec{H} or \vec{D} eigenproblems, whose constraints are independent of ε . For \vec{k} perturbations, one can employ a transformation by Sipe to derive a corrected higher-order perturbation theory (for *e.g.* the group-velocity dispersion), based on the fact that all of the non-transverse fields lie at $\omega = 0$. Such completeness issues also arise applying the variational theorem (3), as we noted in the previous section: in order for a useful variational bound to apply, one must operate in the constrained (transverse) subspace.

3 Two-dimensional Photonic Crystals

After the identification of one-dimensional band gaps, it took a full century to add a second dimension, and three years to add the third. It should therefore come as no surprise that 2d systems exhibit most of the important characteristics of photonic crystals, from nontrivial Brillouin zones to topological sensitivity to a minimum index contrast, and can also be used to demonstrate most proposed photonic-crystal devices. The key to understanding photonic crystals in two dimensions is to realize that the fields in 2d can be divided into two polarizations by symmetry: *TM* (transverse magnetic), in which the magnetic field is in the (xy) plane and the electric field is perpendicular (z); and *TE* (transverse electric), in which the electric field is in the plane and the magnetic field is perpendicular.

Corresponding to the polarizations, there are two basic topologies for 2d photonic crystals, as depicted in Fig. 4(top): high index rods surrounded by low index (top) and low-index holes in high index (bottom). Here, we use a hexagonal lattice because, as noted earlier, it gives the largest gaps. Recall that a photonic band gap requires that the electric field lines run along thin veins: thus, the rods are best suited to TM light (\vec{E} parallel to the rods), and the holes are best suited to TE light (\vec{E} running around the holes). This preference is reflected in the band diagrams, shown in Fig. 4, in which the rods/holes (top/bottom) have a strong TM/TE band gap. For these diagrams, the rod/hole radii is chosen to be $0.2a/0.3a$, where a is the lattice constant (the nearest-neighbor periodicity) and the high/low ε is 12/1. The TM/TE band gaps are then 47%/28% as a fraction of mid-gap frequency, but these band gaps require a minimum ε contrast of 1.7/1 and 1.9/1, respectively. Moreover, it is conventional to give the frequencies ω in units of $2\pi c/a$, which is equivalent to a/λ (λ being the vacuum wavelength)—Maxwell’s equations are scale-invariant, and the same solutions can be applied to any wavelength simply by choosing the appropriate a . For example, the TM mid-gap ω in these units is 0.36, so if one wanted this to correspond to $\lambda = 1.55\mu m$ one would use $a = 0.36 \cdot 1.55\mu m = 0.56\mu m$.

The Brillouin zone (a hexagon) is shown in the inset, with the irreducible Brillouin zone shaded (following the sixfold symmetry of the crystal); the corners (high symmetry points) of this zone are given canonical names, where Γ always denotes the origin $\vec{k} = 0$, K is the nearest-neighbor direction, and M is the next-nearest-neighbor direction. The Brillouin zone is a two-dimensional region of wavevectors, so the bands $\omega_n(\vec{k})$ are actually surfaces, but in practice the band extrema almost always occur along the boundaries of the irreducible zone (*i.e.* the high-symmetry directions). So, it is conventional to plot the bands only along these zone boundaries in order to identify the band gap, as is done in Fig. 4.

Actually, the hole lattice can display not only a TE gap, but a *complete* photonic band gap (for both polarizations) if the holes are sufficiently large (nearly touching). In this case, the thin veins between nearest-neighbor holes induce a TE gap, while the interstices between triplets of holes form “rod-like”

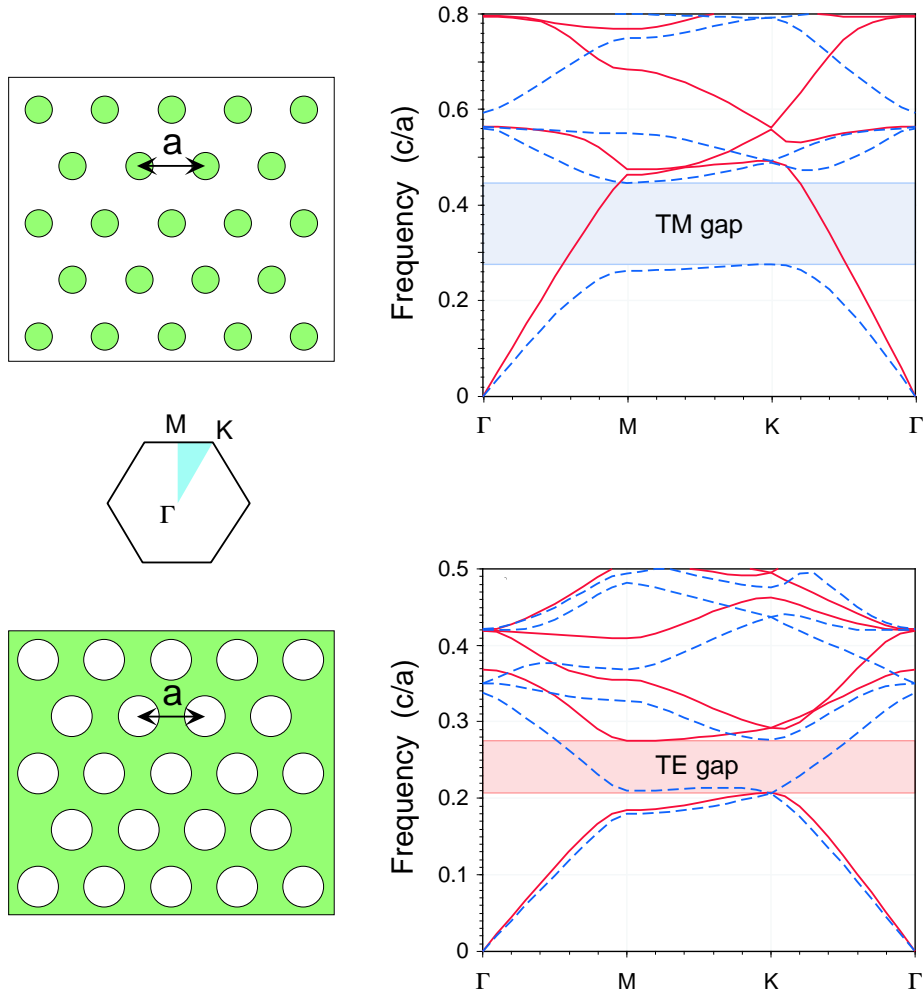


Figure 4: Band diagrams and photonic band gaps for hexagonal lattices of high dielectric rods ($\epsilon = 12$, $r = 0.2a$) in air (top), and air holes ($r = 0.3a$) in dielectric (bottom), where a is the center-center periodicity. The frequencies are plotted around the boundary of the irreducible Brillouin zone (shaded triangle, left center), with solid-red/dashed-blue lines denoting TE/TM polarization (electric field parallel/perpendicular to plane of periodicity). The rods/holes have a gap the TM/TE bands.

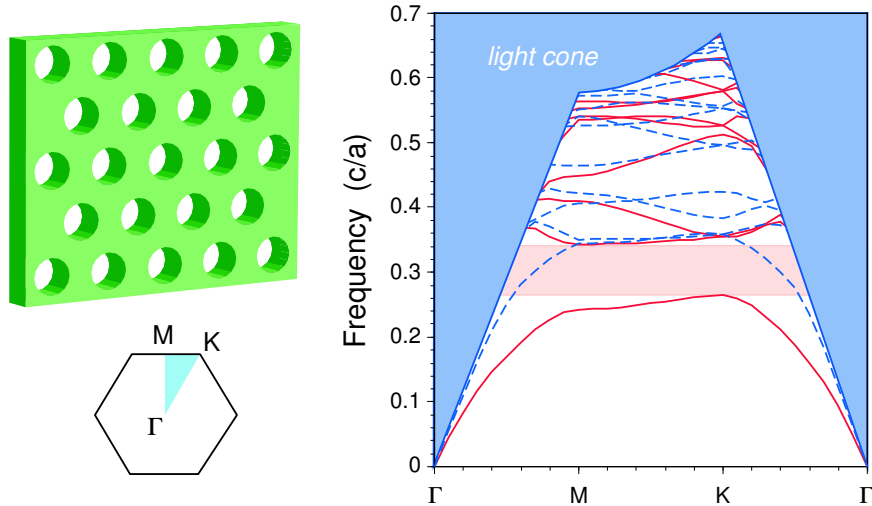


Figure 5: Projected band diagram for a finite-thickness ($0.5a$) slab of air holes in dielectric (cross section as in Fig. 4 bottom), with the irreducible Brillouin zone at lower left. The shaded blue region is the light cone: the projection of all states that can radiate in the air. Solid-red/dashed-blue lines denote guided modes (confined to the slab) that are even/odd with respect to the horizontal mirror plane of the slab, whose polarization is TE-like/TM-like, respectively. There is a “band gap” (region without guided modes) in the TE-like guided modes only.

regions that support a TM gap overlapping the TE gap.

4 Photonic-crystal Slabs

In order to realize 2d photonic-crystal phenomena in three dimensions, the most straightforward design is to simply fabricate a 2d-periodic crystal with a finite height: a photonic-crystal slab, as depicted in Fig. 5. Such a structure can confine light vertically within the slab via *index guiding*, a generalization of total internal reflection—this mechanism is the source of several new tradeoffs and behaviors of slab systems compared to their 2d analogues.

The key to index guiding is the fact that the 2d periodicity implies that the 2d Bloch wavevector \vec{k}_{\parallel} is a conserved quantity, so the *projected band structure* of all states in the bulk substrate/superstrate versus their in-plane wavevector component creates a map of what states can radiate vertically. If the slab is suspended in air, for example, then the eigensolutions of the bulk air are $\omega = c\sqrt{|\vec{k}_{\parallel}|^2 + k_{\perp}^2}$,

which when plotted vs. \vec{k}_{\parallel} forms the continuous *light cone* $\omega \geq c|\vec{k}_{\parallel}|$, shown as a shaded region in Fig. 5. Because the slab has a higher ε (12) than the air (1), it can pull down discrete *guided bands* from this continuum—these bands, lying beneath the light cone, cannot couple to any vertically radiating mode by the conservation law and so are confined to the slab (exponentially decaying away from it). If the horizontal mid-plane of the slab is a mirror symmetry plane, then just as there were TM and TE states in 2d, here there are two categories of modes: *even* (TE-like) and *odd* (TM-like) modes under reflections through the mirror plane (which are purely TE/TM in the mirror plane itself). Because the slab here is based on the 2d hole crystal, which had a TE gap, here there is a 26% “band gap” in the even modes: a range of frequencies in which there are no guided modes. It is not a complete photonic band gap, not only because of the odd modes, but also because there are radiating (light cone) modes at every ω . The presences of these radiating modes means that if translational symmetry is completely broken, say by a waveguide bend or a resonant cavity, then vertical radiation losses are inevitable; there are various strategies to minimize the losses to tolerable levels, however. On the other hand, if only one direction of translational symmetry is broken, as in a linear-defect waveguide, ideally lossless guiding can be maintained.

Photonic-crystal slabs have two new critical parameters that influence the existence of a gap. First, it must have mirror symmetry in order that the gaps in the even and odd modes can be considered separately—such mirror symmetry is broken by the presence of an asymmetric substrate, but in practice the symmetry breaking can be weak if the index contrast is sufficiently high (so that the modes are strongly confined in the slab). Second, the height of the slab must not be too small (or the modes will be weakly confined) or too large (or higher-order modes will fill the gap); the optimum height is around half a wavelength (relative to an averaged index that depends on the polarization). In Fig. 5, a height of $0.5a$ is used, which is near the optimum (with holes of radius $0.3a$ and $\varepsilon = 12$ as in the previous section).

5 Three-dimensional Photonic Crystals

Photonic-crystal slabs are one way of realizing 2d photonic-crystal effects in three dimensions; an example of another way, lifting the sacrifices imposed by the light cone, is depicted in Fig. 6. This is a 3d-periodic crystal, formed by an alternating hole-slab/rod-slab sequence in an ABCABC stacking of bilayers—equivalently, it is an fcc (face-centered cubic) lattice of air cylinders in dielectric, stacked and oriented in the 111 direction, where each overlapping layer of cylinders forms a rod/hole bilayer simultaneously. Its band diagram is shown in Fig. 6 along the boundaries of its irreducible Brillouin zone (from a truncated octahedron, inset), and this structure has a 21%+ complete gap ($\Delta\omega$ as a fraction of mid-gap frequency) for $\varepsilon=12/1$, forbidding light propagation for all wavevectors (directions) and all polarizations. Not only can this crystal confine light perfectly in 3d, but because its layers resemble 2d rod/hole crystals, it turns out

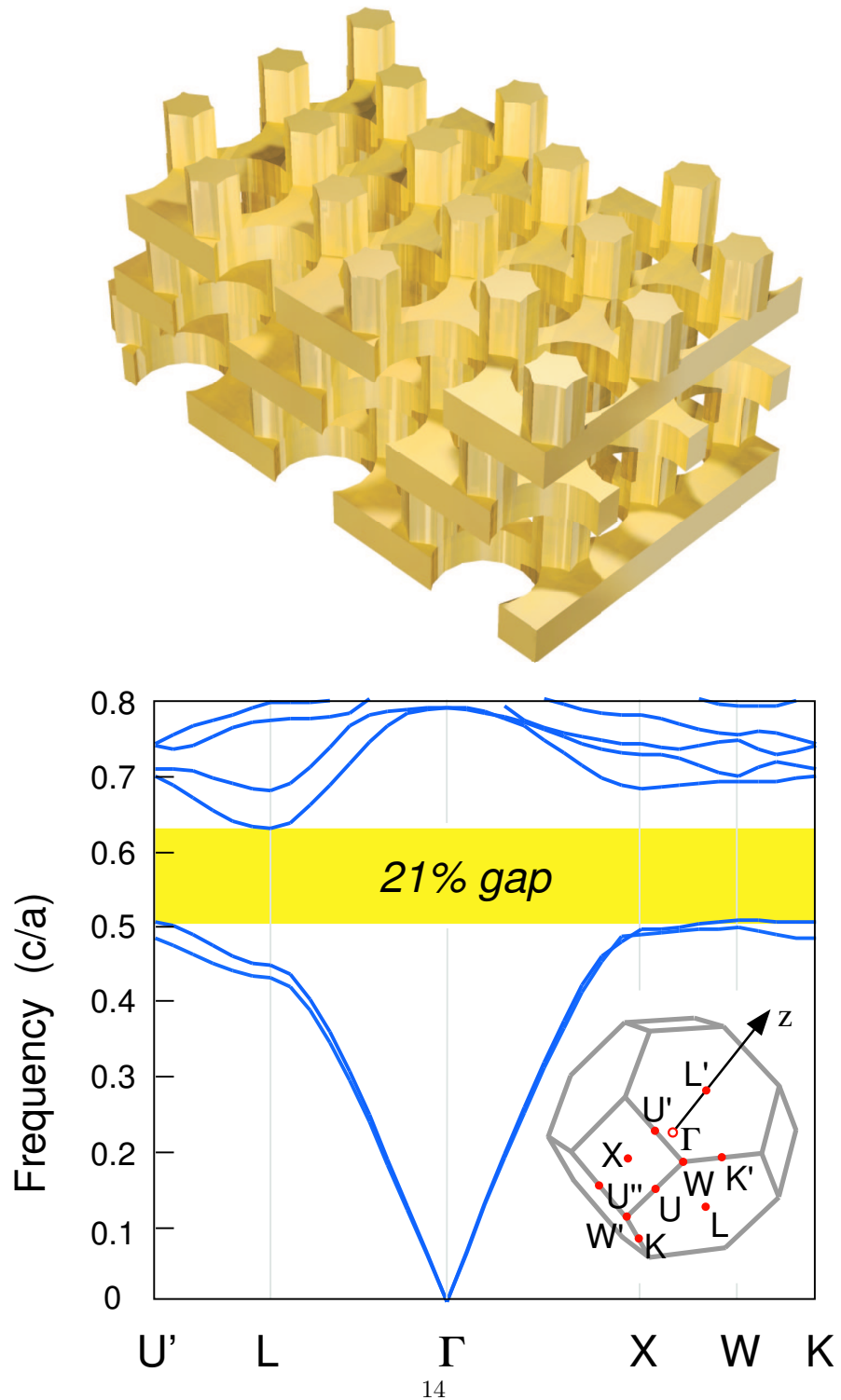


Figure 6: Band diagram (bottom) for 3d-periodic photonic crystal (top) consisting of an alternating stack of rod and hole 2d-periodic slabs (similar to Fig. 4), with the corners of the irreducible Brillouin zone labeled in the inset. This structure exhibits a 21% omnidirectional band gap.

that the confined modes created by defects in these layers strongly resemble the TM/TE states created by corresponding defects in two dimensions. One can therefore use this crystal to directly transfer designs from two to three dimensions while retaining omnidirectional confinement. Its fabrication, of course, is more complex than that of photonic-crystal slabs (with a minimum ε contrast of 4/1), but this and other 3d photonic crystal structures have been constructed even at micron (infrared) lengthscales, as described below.

There are three general dielectric topologies that have been identified to support complete 3d gaps: diamond-like arrangements of high dielectric “atoms” surrounded by low dielectric, which can lead to 20%+ gaps between the 2nd and 3rd bands for $\varepsilon=12/1$ (Si:air) contrast; fcc “inverse opal” lattices of nearly-tangent low dielectric spheres (or similar) surrounded by high dielectric, giving gaps around 10% between the 9th and 10th bands for $\varepsilon=12/1$; and cubic “scaffold” lattices of rods along the cube edges, giving $\sim 7\%$ gaps between the 2nd and 3rd bands for $\varepsilon=12/1$. It is notable that the first two topologies correspond to fcc (face-centered cubic) lattices, which have the most nearly spherical Brillouin zones in accordance with the rules of thumb given above. Many variations on these topologies continue to be proposed—for example, the structure of Fig. 6 is diamond/graphite-like—mainly in conjunction with different fabrication strategies, of which we will mention three successful approaches. First, *layer-by-layer* fabrication, in which individual crystal layers (typically of constant cross-section) are deposited one-by-one and etched with a 2d pattern via standard lithographic methods (giving fine control over placement of defects, *etc.*); Fig. 6 can be constructed in this fashion (as well as other diamond-like structures with large gaps). Second, *colloidal self-assembly*, in which small dielectric spheres in a fluid automatically arrange themselves into close-packed (fcc) crystals by surface forces—these crystals can be back-filled with a high-index material, out of which the original spheres are dissolved in order to form inverse-opal crystals with a complete gap. Third, holographic lithography, in which a variety of 3d crystals can be formed by an interference pattern of four laser beams to harden a light-sensitive resin (which is then back-filled and dissolved, as with colloids, to achieve the requisite index contrast). The second and third techniques are notable for their ability to construct large-scale 3d crystals (thousands of periods) in a short time.

Further Reading

- Ashcroft NW and Mermin ND (1976) *Solid State Physics*. Philadelphia: Holt Saunders.
- Cohen-Tannoudji C, Diu B, and Laloë F. (1977) *Quantum Mechanics*. Paris: Hermann.
- Joannopoulos JD, Meade RD, and Winn JN (1995) *Photonic Crystals: Molding the Flow of Light*. Princeton: Princeton University Press.

- Johnson SG and Joannopoulos JD (2002) *Photonic Crystals: The Road from Theory to Practice*. Boston: Kluwer.
- Johnson SG, Ibanescu M, Skorobogatiy M, Weisberg O, Joannopoulos JD, and Fink Y (2002) “Perturbation theory for Maxwell’s equations with shifting material boundaries,” *Phys. Rev. E*, 65, 066611.
- Sakoda K (2001) *Optical Properties of Photonic Crystals*. Berlin: Springer.
- Sipe JE (2000) “Vector $k \cdot p$ approach for photonic band structures,” *Phys. Rev. E*, 62, 5672–5677.